Numerical Investigation into the Chemistry Induced by Hydrodynamic Cavitation

ARTICLE *in* INDUSTRIAL & ENGINEERING CHEMISTRY RESEARCH · JANUARY 2006

Impact Factor: 2.59 · DOI: 10.1021/ie050839t

Numerical Investigation into the Chemistry Induced by Hydrodynamic Cavitation

J. Sangeeth Krishnan, Prashant Dwivedi, and Vijayanand S. Moholkar*

Chemical Engineering Group, Birla Institute of Technology and Science (BITS), Pilani, Pilani−333 031, Rajasthan, India

The chemical effects induced by acoustic cavitation (popularly known as sonochemical effects) in aqueous medium are well-known and are attributed to the production of various radicals during bubble collapse. Under the influence of pressure variation due to acoustic wave, the bubble expands with the evaporation of water at the gas−liquid interface. This water vapor condenses at the gas−liquid interface during compression. At the final moments of bubble collapse, the dynamics of bubble motion is far more rapid than the diffusion dynamics of water vapor. Therefore, not all the water vapor that has entered the bubble during expansion escapes during compression. The entrapped water molecules are subjected to extremely high temperature and pressure reached during bubble collapse and undergo cleavage to produce various radicals. These radicals are then mixed with the bulk, where they induce various chemical reactions. Similar chemical effects have also been demonstrated by hydrodynamic cavitation, produced because of bubble oscillation and collapse driven by pressure variation in liquid flow. In this work, we try to give a numerical explanation to the sonochemical effects induced by hydrodynamic cavitation. Using a simplified ordinary differential equation (ODE) model for the dynamics of argon bubbles (released because of pressure reduction in the flow) with associated heat and mass transfer, we show that the phenomena of water vapor entrapment and cleavage due to extremes of temperature and pressure at bubble collapse also occur in hydrodynamic cavitation. We also try to investigate the effect of several operating parameters on the extent of water vapor entrapment, the extreme conditions of pressure and temperature generated in the bubble during collapse, and the production of radicals.

1. Introduction

The chemical reactions induced and accelerated by acoustic cavitation due to the passage of ultrasound (termed as *sonochemistry*) are well-known.[1−3] Ultrasound passes through the liquid medium in a series of compression and rarefaction cycles that gives rise to areas of high and low local pressures. Under the influence of varying local pressure, existing gas nuclei in the liquid medium undergo intense volume oscillations. During the expansion phase of volume oscillations, when the pressure at the gas−liquid interface falls below the saturation vapor pressure, evaporation occurs and vapor diffuses into the bubble. During the subsequent collapse phase, liquid vapor tends to condense at the bubble wall. However, during extremely rapid transient bubble collapse (where the bubble wall velocity reaches close to or even exceeds the velocity of sound in liquid), the vapor at the center of the bubble has insufficient time to escape. This excess vapor is, therefore, trapped or *frozen* in the bubble, at the time of minimum radius reached during collapse, when the temperature and pressure inside the bubble is at the extreme (∼5000 K and ∼500 atm). At these conditions, the vapor inside the bubble can decompose to yield radicals such as $H^{\bullet}$, $OH^{\bullet}$, and $HOO^{\bullet}$. These radicals get mixed with the bulk liquid when the bubble fragments during transient collapse and induce various chemical reactions. This is the well-known "sonochemical effect". Many previous studies have tried to give a theoretical explanation of this phenomenon, as discussed in greater detail in the next section.

Hydrodynamic cavitation has been attempted in recent years as an alternative to acoustic cavitation. It can be generated by throttling the liquid flow through simple geometries such as orifice plates. One of the model reactions used in the study of sonochemical effect induced by hydrodynamic cavitation is the oxidation of potassium iodide (KI) resulting in the liberation of iodine.[4−6] An accepted mechanism for this reaction is as follows:[7]

$$2KI + 2OH^{\bullet} \rightarrow 2KOH + I_2$$

$$2HOO^{\bullet} + 2KI \rightarrow 2KOH + I_2 + O_2$$

$$2O^{\bullet} + 2I^{-} + 2K^{+} + 2H_2O \rightarrow I_2 + O_2 + 2KOH + H_2$$

Thus, the radicals produced during the bubble collapse are responsible for the reaction. The purpose of the present study is to give a theoretical explanation of the sonochemistry induced by hydrodynamic cavitation. We try to prove that the phenomena of water vapor entrapment and radical formation occur in hydrodynamic cavitation as well, which is responsible for the sonochemical effect.

2. Water Vapor Entrapment in Cavitation Bubbles: Mechanism and Models

Although it is well-known that the species inducing *sonochemistry*, i.e., radicals such as $OH^{\bullet}$, $H^{\bullet}$, and $HOO^{\bullet}$, are generated during bubble collapse, a direct quantitative measurement of the radical generation is still not possible. This is a principal problem in the sonochemistry research. The variable that has a crucial impact on the state of the bubble interior is temperature, which is obtained by the bubble dynamics equation. During radial motion, the composition inside the bubble varies continuously because of several phenomena such as gas diffusion, gas rectification, water vapor condensation/evaporation, and chemical reactions. If one includes all these aspects into the bubble dynamics model, the problem becomes quite arduous. An approximate, yet physically realistic, attempt to understand these

* To whom correspondence should be addressed. Present address: Department of Chemical Engineering, Indian Institute of Technology Guwahati, North Guwahati, Guwahati−781 039, Assam, India.

10.1021/ie050839t CCC: $33.50
Published on Web 01/11/2006

intricate phenomena requires addressing the above-mentioned aspects step by step. In the following paragraphs, we describe various facets of the physical phenomenon that we try to model, i.e., water vapor entrapment in the cavitation bubbles, along with a review of the published literature, which has dealt with this matter.

Water vapor entrapment in the bubble and its consequences (i.e., chemical reactions, alteration of heat transfer across the bubble) is a subject of active research in the last one and a half decades. Several authors have addressed this problem with different approaches.[8−19]

Kamath et al.[8] estimated the production of OH radicals by decoupling the bubble dynamics equation and the chemical kinetics. Prasad Naidu et al.[9] modeled the equilibrium production of various radicals using the Rayleigh−Plesset equation for the radial motion of the bubble, coupled with Flynn's assumption[20] that the bubble becomes a closed system during collapse, when the partial pressure of gas becomes equal to the vapor pressure. The growth phase of the bubble was assumed to be isothermal, while the collapse phase, after the bubble becomes a closed system, was assumed to be adiabatic. Gong and Hart[13] also took a similar approach of coupling bubble dynamics with the chemical kinetics and explained some trends in sonochemistry. Sochard et al.[10] modeled radical production in mildly forced bubbles, taking into account nonequilibrium phase change and gas-vapor interdiffusion. Like earlier authors, Sochard et al.[10] also assumed the prevalence of equilibrium conditions inside the bubble. Moss et al.[16] performed numerical simulations of the bubble motion, by keeping the amount of water vapor in the bubble constant and uniform during the acoustic cycle and without taking into account the chemical reactions. The principal conclusion of the study of Moss et al.[16] was that inclusion of water vapor in the bubble interior leads to a smaller adiabatic exponent that reduces the heating of the bubble, decreasing the final temperature attained therein. Yasui[11,12] accounted for the nonequilibrium phase change and chemical reactions in a collapsing air bubble. He used a Rayleigh−Plesset type equation for the bubble radius, with the water vapor transport by condensation−evaporation. Also taken into account as per the approach of Kamath et al.[8] were 25 reactions of radicals formed out of water vapor dissociation. However, Yasui[11,12] assumed that transport of water vapor was condensation-limited, i.e., mass diffusion was assumed to be instantaneous and was not explicitly modeled. The primary outcome of Yasui's study was that some water vapor remains in the bubble even at the collapse. With intense heating of the bubble during the transient collapse, this water vapor undergoes endothermic dissociation, reducing the final temperature peak reached in the bubble.

In a landmark paper published in 2000, Storey and Szeri[17] presented a general treatment of the problem, relaxing several assumptions made in earlier studies. The Navier−Stokes equations for the gas mixture in the bubble were coupled to the reaction mechanism. The transport properties (thermal and mass diffusion and viscosity) were calculated from the equations based on the Chapman−Enskog theory, and the equation of state was of the Redlich−Kwong−Soave type. The rate of transport of water molecules was proportional to the difference between the partial pressure of water in the bubble and the saturation pressure at the interface. However, not all the water molecules that approach the surface stick to it, giving rise to nonequilibrium phase change. The fraction of water molecules that stick to the surface is the accommodation coefficient (σ_a). In other words, σ_a is a representative of the resistance to condensation at the interface during bubble collapse. The lower the value of σ_a, the greater this resistance and the higher the amount of water vapor entrapped. Storey and Szeri[17] used the value of $\sigma_a = 0.4$, following the results of Yasui[11] and Eames et al.[21] The principal result of the study by Storey and Szeri[17] was that water vapor transport in the bubble is a two-step process: diffusion to bubble wall and condensation. Thus, it is influenced by two time scales, viz. time scale of diffusion (t_{diff}) and time scale of condensation (t_{cond}), and their magnitudes relative to bubble dynamics (or oscillations) time scale, t_{osc}. In the earlier phases of bubble collapse, $t_{osc} \gg t_{diff}$, t_{cond}, which results in uniform bubble composition. As the bubble wall acceleration increases during collapse, the time scales for bubble dynamics and diffusion become equal. At this stage, the rate of reduction of water vapor in the central region of bubble is less than that at the bubble wall. With further acceleration of the bubble wall, $t_{osc} \ll t_{diff}$, and the water vapor has insufficient time to diffuse to the bubble wall, which results in a nearly fixed distribution of water vapor in the bubble. Another mechanism, which traps water vapor in the bubble during collapse, is the nonequilibrium phase change at the bubble wall, as mentioned above. The time scale for the condensation varies inversely with σ_a. Qualitatively, when $t_{osc} \gg t_{cond}$, the condensation is in equilibrium with respect to the bubble motion. On the other hand, when $t_{cond} \gg t_{osc}$, no water vapor can escape the bubble during collapse. Thus, the amount of water vapor trapped is sensitive to the value of σ_a. There is some disagreement about the value of σ_a, which affects the overall physics of water vapor entrapment, as discussed later in this section.

The exact mechanism by which water vapor is trapped in the bubble is determined by the relative magnitudes of t_{osc}, t_{diff}, and t_{cond}. When the bubble dynamics time scale is smaller than either the diffusion or condensation time scale, water vapor entrapment occurs. However, both mechanisms can contribute to the water vapor entrapment. Storey and Szeri[17] showed that the condition $t_{osc} \ll t_{diff}$ is reached well before $t_{osc} \ll t_{cond}$. Thus, the water vapor trapping is diffusion-limited. Parallel studies conducted by Hoffmann & co-workers (Colussi et al.[14] and Colussi & Hoffmann[15]) clearly show the effect of the condensation time scale that varies inversely with the accommodation coefficient, as mentioned earlier. In their first paper, Hoffmann & co-workers[14] used a very low value of $\sigma_a = 0.001$, without accounting for the finite rate of mass diffusion. With such an unrealistically low value of σ_a, the condition $t_{osc} \ll t_{cond}$ is reached well before $t_{osc} \ll t_{diff}$. This makes the water vapor trapping condensation-limited rather than diffusion-limited. In another study, Colussi and Hoffmann[15] used a value of $\sigma_a = 0.3$, taking into account diffusive resistance generated in the bubble. With this value, the simulation results of Colussi and Hoffmann[15] are in accordance with those of Storey and Szeri[17] that the water vapor trapping is diffusion-limited.

In view of the results of Storey and Szeri[17] with full numerical simulations, Toegel et al.[19] developed a simple diffusion-limited model using boundary layer approximation. This model forms the basis of the present study. The existence of a boundary layer near the bubble wall even at the moment of extremely rapid collapse has been confirmed in the studies of Kwak and co-workers.[22−24] In their analytical calculations of the conservation of mass, energy, and momentum in the bubble, Kwak & co-workers[22−24] showed that the spatial variation of temperature in the bubble was negligible except at the bubble wall. Other authors (Fujikawa & Akamatsu[25] and Kamath et al.[8]) have also justified the existence of the boundary layer. For the validation of the simple model, Toegel et al.[19] have compared their results with those of Storey & Szeri,[17] finding an excellent qualitative

Table 1. Rate Constants for Various Radical Reactions

(A) Parameters for Arrhenius Equation for Specific Reaction Rate[a]

		forward reaction			backward reaction		
no.	reaction	A	c	E_a/k	A	c	E_a/k
1	$O + O + M \leftrightarrow O_2 + M$	1.2×10^{17}	−1	0	3.16×10^{19}	−1.3	59893
2	$O + H + M \leftrightarrow OH + M$	5.0×10^{17}	−1	0	3.54×10^{17}	−0.9	51217
3	$O + H_2 \leftrightarrow H + OH$	3.87×10^{4}	2.7	3150	1.79×10^{4}	2.7	2200
4	$H + O_2 \leftrightarrow O + OH$	2.65×10^{16}	−0.7	8576	1.2×10^{17}	−0.3	−83
5	$H + H + M \leftrightarrow H_2 + M$	1.0×10^{18}	−1	0	1.2×10^{17}	−0.8	52177
6	$H + OH + M \leftrightarrow H_2O + M$	2.2×10^{22}	−2	0	1.2×10^{17}	−2	59980
7	$OH + H_2 \leftrightarrow H + H_2O$	2.16×10^{8}	1.5	1726	1.2×10^{17}	1.3	9529
8	$OH + OH \leftrightarrow O + H_2O$	3.57×10^{4}	2.4	1062	1.2×10^{17}	2.2	7693

(B) Specific Reaction Rate at Various Temperatures

		$T = 1000$ K		$T = 2000$ K		$T = 3000$ K	
no.	reaction	k_f	k_b	k_f	k_b	k_f	k_b
1	$O + O + M \leftrightarrow O_2 + M$	1.2×10^{14}	3.877×10^{-11}	6.0×10^{13}	159.5	4.0×10^{13}	2.04×10^{6}
2	$O + H + M \leftrightarrow OH + M$	5×10^{14}	4.034×10^{-8}	2.5×10^{14}	2.86×10^{3}	1.67×10^{14}	1.01×10^{7}
3	$O + H_2 \leftrightarrow H + OH$	2.088×10^{11}	2.497×10^{11}	6.55×10^{12}	4.87×10^{12}	3.31×10^{13}	2.1×10^{13}
4	$H + O_2 \leftrightarrow O + OH$	3.97×10^{10}	1.231×10^{13}	1.78×10^{12}	9.59×10^{12}	5.59×10^{12}	8.38×10^{12}
5	$H + H + M \leftrightarrow H_2 + M$	1.0×10^{15}	6.495×10^{-8}	5.0×10^{14}	7.97×10^{3}	3.33×10^{14}	3.5×10^{7}
6	$H + OH + M \leftrightarrow H_2O + M$	2.2×10^{16}	3.279×10^{-9}	5.5×10^{15}	8.67×10^{3}	2.44×10^{15}	8.46×10^{7}
7	$OH + H_2 \leftrightarrow H + H_2O$	1.216×10^{12}	3.003×10^{9}	8.15×10^{12}	8.67×10^{11}	1.99×10^{13}	7.19×10^{12}
8	$OH + OH \leftrightarrow O + H_2O$	1.636×10^{12}	1.519×10^{16}	5.08×10^{12}	1.49×10^{15}	1.13×10^{13}	1.01×10^{15}

[a] Note: The above parameters (part A) correspond to the specific reaction rate constant equation $k_r = AT^c \exp[(-E_a)/(kT)]$. Units of A are either $cm^3\ mol^{-1}\ s^{-1}$ (two-species reaction) or $cm^6\ mol^{-2}\ s^{-1}$ (three-species reaction). E/k is the activation temperature in K. Data are taken from ref 40.

and quantitative agreement. This is another confirmation that the water vapor transport is diffusion-limited rather than condensation-limited.

3. Aim and Approach of Present Study

The present study aims at discerning the mechanism of sonochemistry induced by hydrodynamic cavitation, which can be generated by the throttling of flow through confined geometries such as an orifice. Modeling of this phenomenon would require the combining of bubble dynamics formulation with the hydrodynamics of a complex turbulent flow field downstream from an orifice. A detailed modeling of the turbulent flow field requires direct numerical simulation (DNS), which is an enormously intensive procedure. Several other models are available for the turbulent flows, such as the popular $k-\epsilon$ model, which averages out the Reynolds stresses in the flow. However, with the coupling of detailed bubble dynamics formulation, even these models pose a highly arduous problem. Moreover, the process of radical formation in the bubble is a result of several vapor-phase reactions for which the kinetics need to be taken into account.

In view of these difficulties and complexities, we make two approximations in our approach, described as follows:

1. A reduced algorithm for the estimation of turbulent velocity fluctuations, which is based on Kolmogoroff's hypothesis that the rate at which large eddies supply energy to the smaller eddies is proportional to the reciprocal of the time scale of larger eddies. Moreover, we consider only axial velocity fluctuations in our calculations (neglecting radial and azimuthal fluctuations). This approximation is based on the measurements of the turbulent velocity field downstream from an orifice by Morrison et al.,[26] which shows that the axial variance (or mean square of axial velocity fluctuations) was much higher than the radial and azimuthal variances.

2. The attainment of thermodynamic equilibrium at the bubble collapse, which is based on the relative magnitudes of the bubble-collapse time scale and the time scales of various radical reactions. The time scale of bubble collapse, as determined by Storey and Szeri, is of the order of a few tens of nanoseconds ($\sim 10^{-8}$). For the system considered in this work (argon and water vapor), as many as eight reactions are possible. Table 1B lists the specific rate constants for these reactions calculated from the Arrhenius equation (refer to Table 1A) at temperatures of 1000, 2000, and 3000 K—typical of those attained during the bubble collapse. Moreover, the concentrations in the bubble at the moment of collapse are very high. An order-of-magnitude calculation done with representative numbers [$\sim 10^{10}$ molecules or 10^{-13} moles in a bubble compressed to one-tenth of its original size, which is in the micron (or $\sim 10^{-4}$ cm) range, i.e., $\sim 10^{-5}$ cm] puts concentrations as ~ 100 mol/cm^3. Even with a conservative estimate of concentration, the time scale for the reaction (t_{react}) can be taken as $\sim$1/specific reaction rate. Comparison of the time scale of bubble collapse with the time scale of reactions reveals that the latter is at least 2 orders of magnitude smaller. Thus, thermodynamic equilibrium should prevail till the point of minimum radius during collapse. This justifies our assumption of thermodynamic equilibrium.

We would like to emphasize that our approach addresses the basic physics of the problem; a more rigorous approach relaxing the assumptions/approximations in our model would modify only the final quantitative answers.

4. Mathematical Formulation

As mentioned earlier, we use the model proposed by Toegel et al.[19] as the basis for the present study. We first present the model for bubble dynamics and the associated heat and mass transfer, followed by the model for the orifice flow, which has been used in the previous work of one the authors of this paper.[27,28] The liquid medium in the present study is assumed to be water saturated with a monatomic gas such as argon. We choose these conditions for our simulation on the basis that monatomic gases have been widely used to induce cavitation nuclei in the sonochemical reactions because of their high specific-heat ratio, with water as the liquid medium, owing to its low vapor pressure. In the orifice flow, when the pressure at vena contracta falls because of the rise in velocity, dissolved argon is liberated in the form of small bubbles, which flow along with the liquid flow, undergoing oscillations and collapse with

the pressure recovery. If the liquid pressure falls to the vapor pressure of the liquid at the operating temperature, partial vaporization of the liquid also takes place, resulting in formation of vapor bubbles. However, in the present study, we focus only on the gas bubbles because the vapor bubbles dissolve very rapidly due to the condensation of vapor with rising pressure.

4.1. Bubble Dynamics. The bubble motion is described by the Keller−Miksis equation written as[29,30]

$$\left(1-\frac{\mathrm{d}R/\mathrm{d}t}{c}\right)R\frac{\mathrm{d}^2R}{\mathrm{d}t^2}+\frac{3}{2}\left(1-\frac{\mathrm{d}R/\mathrm{d}t}{3c}\right)\left(\frac{\mathrm{d}R}{\mathrm{d}t}\right)^2=\frac{1}{\rho_\mathrm{L}}\left(1+\frac{\mathrm{d}R/\mathrm{d}t}{c}\right)(P_\mathrm{i}-P_\mathrm{t})+\frac{R}{\rho_\mathrm{L}c}\frac{\mathrm{d}P_\mathrm{i}}{\mathrm{d}t}-4\nu\frac{\mathrm{d}R/\mathrm{d}t}{R}-\frac{2\sigma}{\rho_\mathrm{L}R} \quad (1)$$

where P_t is the time-variant local pressure. Calculation of P_t for an orifice flow is explained later. The pressure inside the bubble P_i is written as

$$P_\mathrm{i}=\frac{N_\mathrm{tot}(t)kT}{\left[\frac{4\pi}{3}(R^3(t)-h^3)\right]^\gamma} \quad (2)$$

where $h \approx R_\mathrm{o}/8.86$ is the van der Waals hard core radius, determined by the excluded volume of gas molecules. Since the excluded volume for both argon and water differs byonly 5%, we take a common hard core radius for both. The exponent γ is the effective polytropic exponent. Plesset and Prosperetti[31] calculated how it depends on the thermal Peclet number $Pe = R_\mathrm{o}^2\omega/\kappa$, which gives the ratio between bubble length scale, R_o, and thermal diffusion length $\sqrt{\kappa/\omega}$. Hilgenfeldt et al.[32] have argued that the frequency ω should be replaced by the bubble dynamics time scale $|\mathrm{d}R/\mathrm{d}t|/R$. With this substitution, the Peclet number becomes as high as 10^4 at the moments of rapid bubble collapse, implying that γ should take the value of the ratio of specific heats. However, the condition for which $Pe \gg 1$ holds only for a very small time interval, ~1 ns. Therefore, global dynamics are not affected by setting $\gamma = 1$ uniformly in time. A noteworthy consequence of this approximation is that isothermal conditions prevail at the bubble wall. This is also supported by the large heat capacity of water. The isothermal condition at the bubble wall is further used in the model for mass transfer across the bubble, described in the next subsection. After substituting $\mathrm{d}R/\mathrm{d}t = s$, the above equation is transformed into two simultaneous equations:

$$\frac{\mathrm{d}R}{\mathrm{d}t}=s \quad (3)$$

$$\frac{\mathrm{d}s}{\mathrm{d}t}=\frac{(1+s/c)}{R\rho_\mathrm{L}(1-s/c)}(P_\mathrm{i}-P_\mathrm{t})+\frac{1}{\rho_\mathrm{L}c(1-s/c)}\frac{\mathrm{d}P_\mathrm{i}}{\mathrm{d}t}-\frac{4\nu s}{R^2(1-s/c)}-\frac{2\sigma}{\rho_\mathrm{L}R^2(1-s/c)}-\frac{3}{2}\frac{s^2(1-s/3c)}{R(1-s/c)} \quad (4)$$

4.2. Mass Transfer Across Bubble. During bubble oscillations, both argon and water vapor diffuse across the bubble wall. However, the time scale of diffusion of argon is much larger than the time scale of bubble oscillations. Therefore, we ignore the diffusion of argon across the bubble wall. Diffusion of the water vapor across the bubble wall shows interesting features, as already discussed in Section 2. During bubble oscillations, the surface temperature of the bubble exceeds bulk water temperature only for a very brief moment during collapse. On this basis, the bubble can be divided into two parts: (i) a "cold" boundary layer in thermal equilibrium with liquid and (ii) a hot homogeneous core. Of course, this distinction is based on the assumption that the condensation of water molecules at the bubble wall is fast enough to maintain equilibrium. By dimensional analysis, the instantaneous diffusive penetration depth is given by $l_\mathrm{diff} = \sqrt{D_{ij}t_\mathrm{osc}}$, where D_{ij} is the binary diffusion coefficient and t_osc is the time scale of bubble oscillations: $|\mathrm{d}R/\mathrm{d}t|/R$. The assumption of the bubble interior divided in two parts mentioned above can be supported by analysis of the diffusive penetration depth: during growth and the major part of compression, $l_\mathrm{diff} \geq R$. This means that the total bubble volume is in equilibrium with the liquid. During the final phase of compression, the bubble wall velocity becomes very high. At these instances, $l_\mathrm{diff} = 0.01R$. The thickness of the boundary layer is negligible compared to the bubble volume, and hence, the bubble can again be treated as a homogeneous core.

On the basis of the results of Storey and Szeri,[17] who conclude that the water vapor transport is always diffusion-limited, and the other approximations stated above, the rate of change of water molecules in the bubble is given by

$$\frac{\mathrm{d}N_\mathrm{W}}{\mathrm{d}t}=4\pi R^2D_{ij}\frac{\partial C_\mathrm{W}}{\partial r}\Big|_{r=R}\approx 4\pi R^2D_{ij}\left(\frac{C_\mathrm{WR}-C_\mathrm{W}}{l_\mathrm{diff}}\right) \quad (5)$$

where C_WR is the equilibrium concentration of water molecules at the bubble wall, calculated using the vapor pressure at the bulk temperature (T_o), and C_W is the actual concentration of water molecules in the bubble core.

4.2.1. Upper Limit on Diffusion Length. The above analysis holds good for a bubble in motion, where the bubble wall velocity, $\mathrm{d}R/\mathrm{d}t$, has a nonzero value. However, at the instances of maximum and minimum radius, the bubble wall velocity is zero, and we need an alternate expression for the diffusion length. For this purpose, we identify that, for $\mathrm{d}R/\mathrm{d}t = 0$, the equation for vapor transport inside the bubble becomes a pure diffusion equation,

$$\frac{\partial C_\mathrm{W}}{\partial t}=D_{ij}\left(\frac{\partial^2 C_\mathrm{W}}{\partial r^2}+\frac{2}{r}\frac{\partial C_\mathrm{W}}{\partial r}\right) \quad (6)$$

with the following boundary conditions: (1) $r = 0$, $\partial C_\mathrm{W}/\partial t = 0$ for $t \geq 0$; (ii) $r = R$, $C_\mathrm{W} = C_\mathrm{WR}$ for $t \geq 0$; and (iii) $C_\mathrm{W} = C_\mathrm{W0} = 0$ for $t = 0$ and $0 \leq r \leq R$. The analytical solution to the above problem is given by Crank:[33]

$$\frac{C_\mathrm{W}-C_\mathrm{W0}}{C_\mathrm{WR}-C_\mathrm{W0}}=1+\frac{2R}{\pi r}\sum_{n=1}^{\infty}\frac{(-1)^n}{n}\sin\left(\frac{nr}{R/\pi}\right)\exp\left(-\frac{n^2D_{ij}t}{(R/\pi)^2}\right) \quad (7)$$

From the inspection of the above solution, the characteristic length for the diffusion is R/π. We choose this as the upper limit for the diffusion length. Thus,

$$l_\mathrm{diff}=\min\left(\sqrt{\frac{RD_{ij}}{|\mathrm{d}R/\mathrm{d}t|}},\frac{R}{\pi}\right) \quad (8)$$

The diffusion coefficient is determined from the equation based on Chapman−Enskog theory using a Lennard-Jones 12−6 potential. Greater details about the diffusion coefficient calculation are given in Appendix A.

4.3. Heat Transfer Across Bubble. With complete analogy with mass transfer, the heat transfer across the bubble wall is

$$\frac{dQ}{dt} = 4\pi R^2 \lambda_{ij} \left(\frac{T_o - T}{l_{th}} \right) \tag{9}$$

where λ_{ij} is the thermal conductivity of the binary (argon−water vapor) mixture and l_{th} is the thermal diffusion length:

$$\min\left(\frac{R}{\pi}, \sqrt{\frac{R\kappa_{ij}}{|dR/dt|}} \right)$$

Thermal diffusivity κ_{ij} is calculated as $\kappa_{ij} = \lambda_{ij}/(\rho_{mix} C_{p,mix})$, where $\rho_{mix} C_{p,mix} = \rho_{Ar} C_{p,Ar} + \rho_W C_{p,W}$. The densities ($\rho_{Ar}$ and ρ_W) are expressed in terms of molecules/m^3, and the molecular specific heats for argon and water are

$$C_{P,Ar} = \frac{5}{2} N_{Ar} k \tag{10}$$

$$C_{p,W} = N_W k \left(4 + \sum \frac{(\theta_i/2T)^2}{\sinh^2(\theta_i/2T)} \right) \tag{11}$$

where θ_i are the characteristic vibrational temperatures for the water molecule. We take the following values for these: $\theta_1 = 2295$ K, $\theta_2 = 5255$ K, and $\theta_3 = 5400$ K (Hirschfelder et al.[34]). As far as the effective thermal conductivity of the argon−water vapor mixture is concerned, we follow a semiempirical method given in Hirschfelder et al.[34] This method is described in Appendix A.

4.4. Overall Energy Balance. Treating the bubble as an open system, the overall energy balance for the bubble contents is written as

$$\frac{dE}{dt} = \frac{dQ}{dt} - \frac{dW}{dt} + h_W \frac{dN_W}{dt} \tag{12}$$

However, the total energy E is a function of the temperature and volume of the bubble and the number of molecules of various species in it. Thus, the rate of change of E can also be written as

$$\frac{dE}{dt} = \left(\frac{\partial E}{\partial N_W} \right)_{N_{Ar},V,T} \frac{dN_W}{dt} + \left(\frac{\partial E}{\partial N_{Ar}} \right)_{N_W,V,T} \frac{dN_{Ar}}{dt} + \left(\frac{\partial E}{\partial T} \right)_{N_w,N_{Ar},V} \frac{dT}{dt} + \left(\frac{\partial E}{\partial V} \right)_{N_W,N_{Ar},T} \frac{dV}{dt} \tag{13}$$

where dN_W/dt and dN_{Ar}/dt are the rate of change of water and argon molecules in the bubble, respectively. Per our assumption, $dN_{Ar}/dt = 0$; hence, we neglect the second term on the right-hand side (RHS). The enthalpy of the water molecule entering the bubble from the "cold" interface is $h_W = 4kT_o$. The specific energy of the water molecule in the bubble is the thermal energy and is written as

$$\left(\frac{\partial E}{\partial N_W} \right) = U_W = NkT \left(3 + \sum \frac{\theta_i/T}{\exp(\theta_i/T) - 1} \right) \tag{14}$$

The work done by the bubble reduces to expansion work: $\Delta W = P_i\, dV$. Comparing eqs 12 and 13, and identifying that $(\partial E/\partial T) = C_v$ and $(\partial E/\partial V) = 0$, as the internal energy of an ideal gas is mainly a function of its composition and temperature, we can now write another equation for the change of the temperature of the bubble:

$$C_{v,mix} \frac{dT}{dt} = \frac{dQ}{dt} - P_i \frac{dV}{dt} + (h_W - U_W) \frac{dN_W}{dt} \tag{15}$$

The specific heat of the mixture $C_{v,mix}$ is written in terms of the molecular specific heats of argon and water and the molecules of argon (N_{Ar}) and water (N_W) present in the bubble,

$$C_{v,Ar} = \frac{3}{2} k N_{Ar} \tag{16}$$

$$C_{v,W} = k \left(3 + \sum \frac{(\theta_i/2T)^2}{\sinh^2(\theta_i/2T)} \right) N_W \tag{17}$$

finally giving

$$C_{v,mix} = C_{v,Ar} + C_{v,W} \tag{18}$$

4.5. Pressure Variation in the Liquid Stream. The flow past an orifice plate in the case of a high *Re* flow has two components: the mean flow velocity (U) and the turbulent fluctuating velocity ($\bar{u}'$). Thus, the instantaneous velocity in the flow downstream of the orifice is written as

$$U_t = U + \bar{u}' \tag{19}$$

The velocity of the mean flow at vena contracta (U_o) can be determined using the cavitation number defined as

$$C_i = \frac{P_2 - P_v}{\left(\frac{1}{2} \rho_L U_o^2 \right)} \tag{20}$$

It is quite clear that, for $C_i = 1$, the pressure at vena contracta falls to the vapor pressure of the liquid at the operating temperature. After calculating U_o for an assumed value of C_i, the velocity in the pipe (U_p) is calculated from the orifice-to-pipe diameter ratio (β) as

$$U_p = \beta^2 U_o \tag{21}$$

The region of pressure recovery downstream of the orifice (L') extends to ∼8−10 pipe diameters. Using the values of L', U_p, and U_o, the time of pressure recovery downstream of the orifice (τ) is calculated using Newton's equations.

To determine the second component of the instantaneous velocity, i.e., $\bar{u}'$, we use an algorithm used in our earlier work,[27,28] which is based on the assumption that the rate at which large eddies supply energy to the smaller eddies is proportional to the reciprocal of the time scale of larger eddies. The amount of kinetic energy per unit mass is proportional to $\bar{u}'^2$, and the rate of energy transfer is assumed to be $\bar{u}'/l$, where l is the size of the largest eddies in the flow. The rate of energy supply is equal to the rate of energy dissipation and is given as $\sim \bar{u}'^2 (\bar{u}'/l) = \bar{u}'^3/l$. The main steps of the algorithm are as follows:

(1) The rate of turbulent energy dissipation per unit mass in the region of pressure recovery downstream of the orifice is estimated using the permanent pressure head loss in the flow and the volumetric flow rate. Moreover, we consider turbulent velocity fluctuations only in axial direction, for the reasons already stated in Section 3.

(2) The length scale of the eddy is estimated using the Prandtl eddy model ($l = 0.08 d_c$), in which the conduit diameter d_c is taken as an average of orifice and pipe diameters.

(3) The steady-state frequency of the turbulent fluctuating velocity, f_T, is obtained by multiplying the rate of energy transfer ($\bar{u}'/l$) by the time of pressure recovery, τ.

4.5.1. Calculation of Instantaneous Bulk Pressure (P_t). Using values of various quantities, U_o, τ, $\bar{u}'$, and f_T, the instantaneous bulk pressure in the flow is calculated as follows:

(1) In consideration of the experimental results of Yan et al.,[35] the instantaneous pressure P_t at any time t is first calculated assuming a linear pressure recovery between the pressure at vena contracta (P_{vc}) and an assumed recovery pressure (P_2) downstream of the orifice:

$$P_t = P_{vc} + \frac{(P_2 - P_{vc})}{\tau} t \tag{22}$$

(2) The instantaneous mean velocity (U_t) corresponding to the above value of P_t is calculated using the Bernoulli equation between vena contracta and the point of full pressure recovery (8 pipe diameters downstream of the orifice):

$$U_t = \left(\frac{P_{ori} + \frac{1}{2}\rho_L U_o^2 - P_t}{\frac{1}{2}\rho_L} \right)^{1/2} \tag{23}$$

(3) The turbulent fluctuation velocity is superimposed over U_t to calculate the new value of the instantaneous velocity as follows:

$$U_t^{new} = U_t + \bar{u}' \sin(2\pi f_T t) \tag{24}$$

(4) The bulk pressure in the flow is recalculated using the Bernoulli equation:

$$P_t = \frac{1}{2}\rho_L U_o^2 + P_{vc} - \frac{1}{2}\rho_L (U_t^{new})^2 \tag{25}$$

The above value of P_t is then substituted in the bubble dynamics equation (eq 4).

4.6. Numerical Solution. Equations 3, 4, 5, and 15 constitute the complete formulation for radial motion of a bubble, which can be solved simultaneously using the Runge−Kutta fourth-order−fifth-order adaptive step-size method (Press et al.[36]) to get the radius history of the bubble along with the instantaneous number of water molecules trapped in the bubble and the temperature of the bubble contents. The initial conditions used for the solution are $t = 0$, $R = R_o$, $dR/dt = 0$, $N_W = 0$, and $T = T_o$. We would like to mention that the phenomenon of bubble collapse (or bubble fragmentation) depends on many factors such as the surface instability, the local flow conditions, and the bubble population in the vicinity of the bubble. For the conditions of maximum surface instability and flow instability, the bubble collapses at first compression after an initial expansion. Considering this, the condition for bubble collapse is taken as the first compression after an initial expansion. However, it is not necessary that the bubble collapse at the first compression. For milder instabilities, it may rebounce and undergo many oscillations, with the recovery of pressure of the liquid flow, as shown in the simulations described in the next section. The equilibrium composition of the various species in the bubble (i.e., H_2O, H_2, O_2, $H^\bullet$, $OH^\bullet$, $O^\bullet$, H_2O_2, $HOO^\bullet$, and O_3) at the conditions of temperature and pressure at the first compression was calculated using the software Factsage, which uses the free-energy minimization algorithm proposed by Eriksson.[37] This software has a built-in database of C_p vs temperature relationship, entropy, and heat of formation of all the above species.

5. Results and Discussion

Simulations of the radial dynamics of the bubble along with associated heat and mass transfer for various parameter sets, given in Table 2, are shown in Figures 1−5. These simulations not only explain the phenomena of radical formation in hydrodynamic cavitation but also help one understand the effect of the various operational parameters. The summary of the simulation results is given in Table 3, which lists the collapse conditions (i.e., the number of water molecules entrapped in the bubble and the temperature and pressure inside the bubble during main or first collapse) and the equilibrium composition of the various species at these conditions.

Figures 1−5 show that a large amount of water vapor enters the bubble during the expansion phase. During extremely rapid collapse, the bubble dynamics time scales become much faster than the mass diffusion time scale, and thus not all the water vapor can escape the bubble. A significant amount of water molecules get entrapped in the bubble and are subjected to extremes of temperatures and pressure at maximum compression. The equilibrium mole fraction of all species calculated

Table 2. Parameters for Simulation[a]

	parameter						
set no.	P_2 (atm)	R_o (μm)	β	C_i	τ (s)	$\bar{u}'$ (m/s)	f_T (kHz)
set 1	1	200	0.5	1	0.0462	1.316	0.432
set 2	1.2	200	0.5	1	0.0421	1.398	0.459
set 3	1	100	0.6	1	0.0425	1.129	0.347
set 4	1	200	0.6	1	0.0425	1.129	0.347
set 5	1	200	0.5	1.1	0.0485	1.316	0.432

[a] A pipe size of 2 in. is taken for all simulations. The liquid temperature is assumed to be 20 °C.

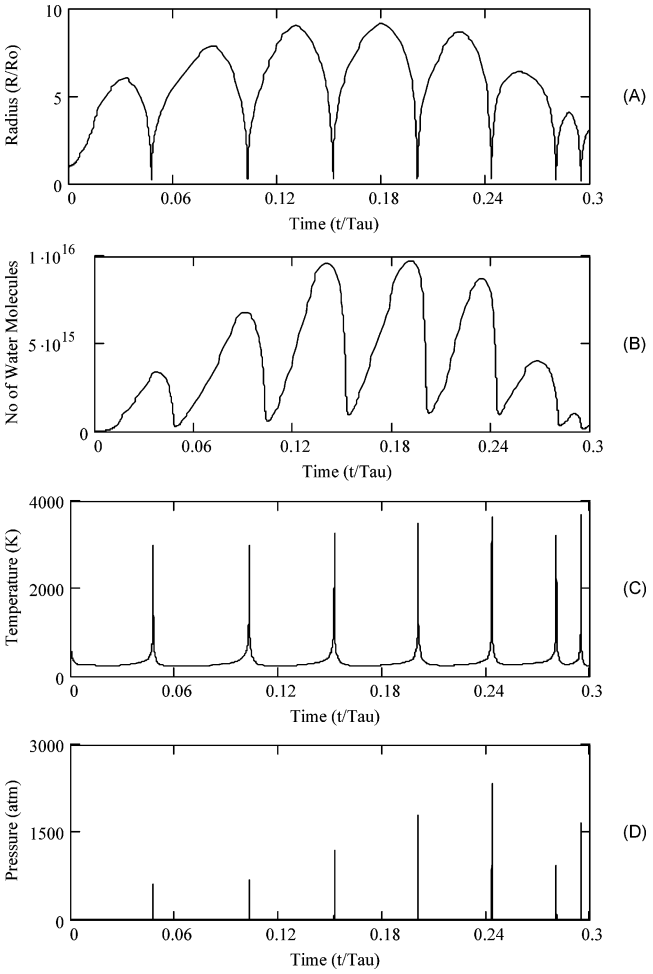

Figure 1. Simulation results for parameter set 1. Time variation of (A) normalized bubble radius (R/R_o); (B) number of water molecules in the bubble; (C) temperature in the bubble; and (D) pressure in the bubble.

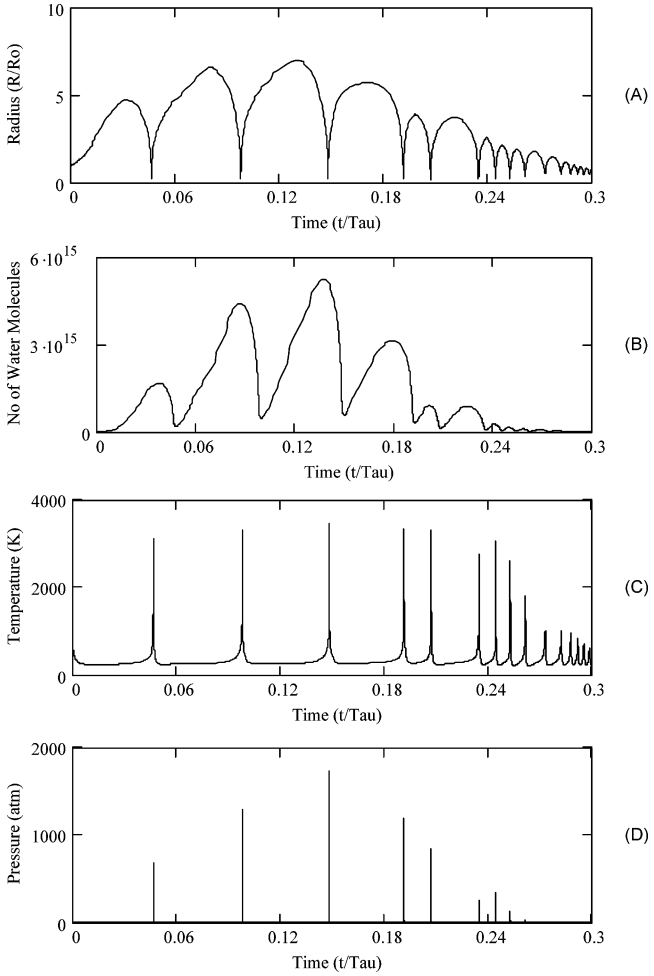

Figure 2. Simulation results for parameter set 2. Time variation of (A) normalized bubble radius (R/R_o); (B) number of water molecules in the bubble; (C) temperature in the bubble; and (D) pressure in the bubble.

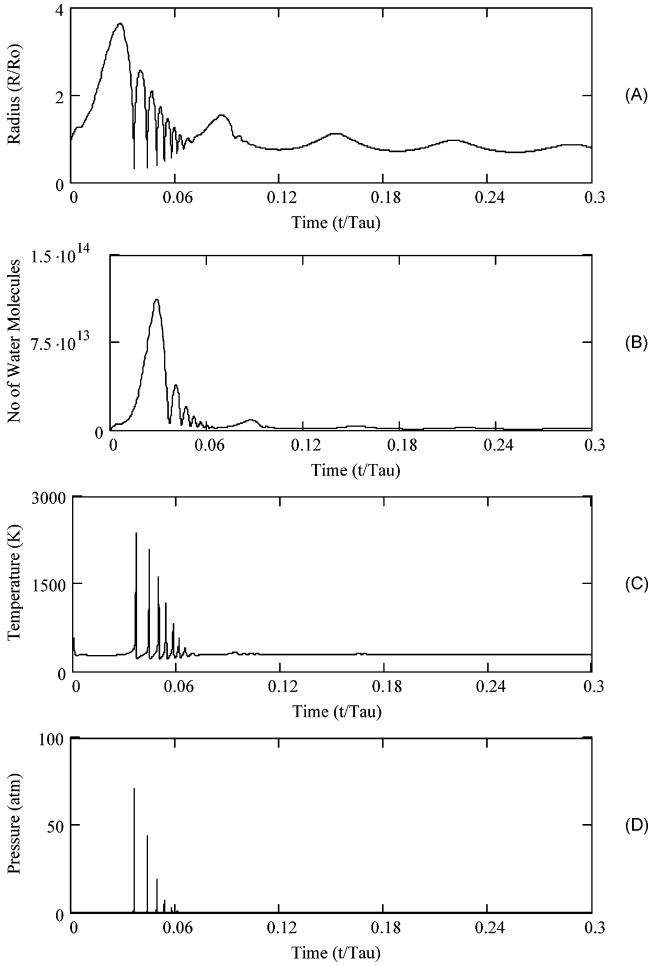

Figure 3. Simulation results for parameter set 3. Time variation of (A) normalized bubble radius (R/R_o); (B) number of water molecules in the bubble; (C) temperature in the bubble; and (D) pressure in the bubble.

using Factsage shows that the dominant radical species is OH• with its equilibrium mole fraction being at least an order of magnitude higher than that of the other species. Quite obviously, these radicals get mixed with the bulk after fragmentation of the bubble and give rise to many chemical reactions.

The effects of various parameters can be found by comparing the simulations shown in different figures. In the orifice flow, the bubble motion (and associated phenomena) are influenced by the sum of two pressure gradients: (1) the mean pressure gradient, $\sim{}^1/_2\rho_L L'(1-\beta^2)U_o^2$, which is linearly increasing, and (2) the turbulent pressure gradient $\sim{}^1/_2\rho_L\bar{u}'^2$, which is oscillatory in nature, as explained earlier. The pressure falls during negative oscillation of the turbulent pressure gradient, due to which the bubble expands. The expansion of the bubble, which is accompanied by the diffusion of water vapor inside it, is proportional to the intensity of the turbulent pressure gradient, which in turn mainly depends on the orifice-to-pipe-diameter ratio. For a given recovery pressure downstream of the orifice plate, the lower the orifice-to-pipe-diameter ratio, the higher is the permanent pressure head loss (and energy dissipation) and the higher is the intensity of turbulent velocity fluctuations. On the other hand, the mean pressure gradient is mainly a function of recovery pressure for a given cavitation number.

5.1. Effect of Recovery Pressure. Comparing Figures 1 and 2 reveals the effect of recovery pressure downstream of the orifice on the water vapor entrapment and the radical formation during radial bubble motion. With rising recovery pressure, both the linear mean pressure gradient and turbulent oscillatory pressure gradients rise. The maximum radius reached during the expansion phase is more-or-less the same in both cases, Figures 1 and 2. However, during the subsequent compression, the mean and turbulent pressure gradients add. Hence, with rising recovery pressure, the compression ratio of the bubble increases. Thus, more water vapor gets squeezed out of the bubble, and the temperatures and pressures reached during the collapse rise. Although at the conditions of higher temperature and pressure the equilibrium fraction of OH• increases, the total amount of radicals produced decreases because of less entrapment of the water vapor at collapse.

5.2. Effect of Orifice-to-Pipe-Diameter Ratio. Comparison of Figures 1 and 4 gives the effect of the orifice-to-pipe-diameter ratio on the bubble dynamics and associated phenomena. With a relatively small rise in the orifice-to-pipe-diameter ratio (from 0.5 to 0.6), sonochemical effects reduce significantly. Not only do the temperatures and pressures reached during the bubble collapse reduce sharply, but the water vapor entrapment also decreases by an order of magnitude. A rise in the orifice-to-pipe-diameter ratio reduces both the intensity and frequency of turbulent velocity fluctuations. Because of the lower intensity of turbulent fluctuations, bubble expansion is reduced. Thus, the amount of water vapor diffusing inside it decreases. Moreover, the lower frequency of turbulent fluctuations increases the time scale of compression, thus increasing the extent of heat and mass transfer during this phase. This results in less water vapor entrapment and lower temperatures and pressures during collapse. Moreover, the equilibrium mole fraction of OH•

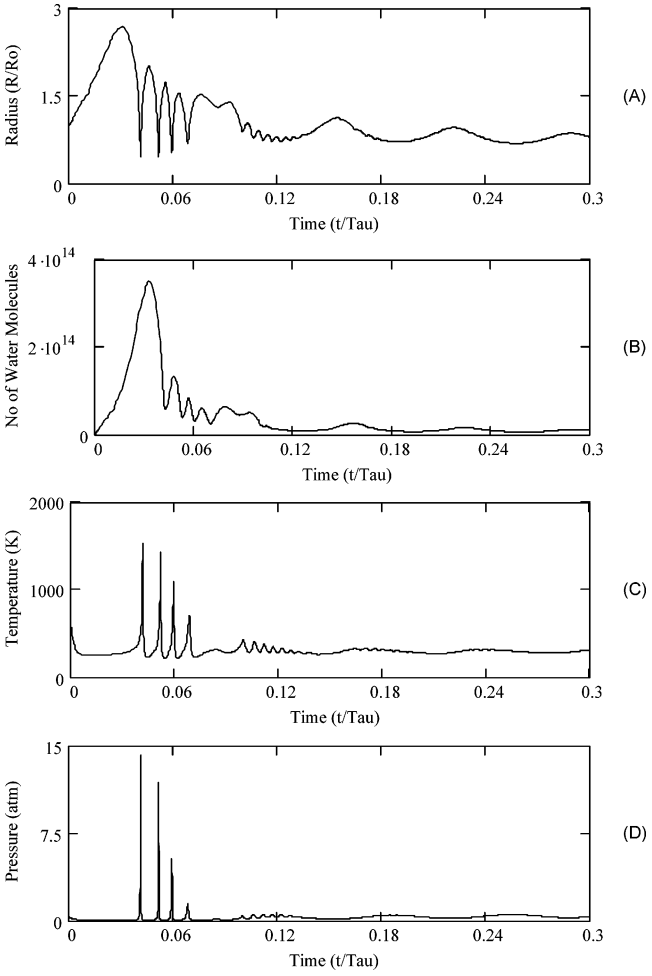

Figure 4. Simulation results for parameter set 4. Time variation of (A) normalized bubble radius (R/R_o); (B) number of water molecules in the bubble; (C) temperature in the bubble; and (D) pressure in the bubble.

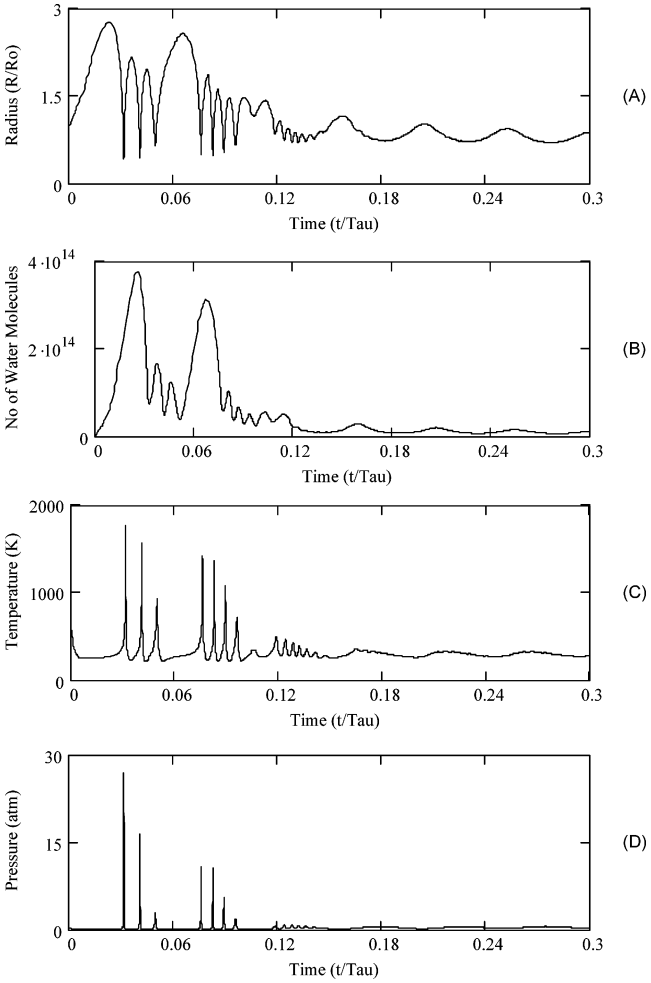

Figure 5. Simulation results for parameter set 5. Time variation of (A) normalized bubble radius (R/R_o); (B) number of water molecules in the bubble; (C) temperature in the bubble; and (D) pressure in the bubble.

radicals at the conditions of collapse reduces by 3 orders of magnitude. As a result of all this, the sonochemical effects reduce significantly with a small rise in orifice-to-pipe-diameter ratio.

5.3. Effect of Initial Bubble Radius. The effect of the initial bubble radius can be found by comparing Figures 3 and 4. A smaller bubble (100 microns) undergoes a greater compression, giving higher values of temperature and pressure at collapse. Moreover, the amount of water vapor entrapped in the bubble is also reduced by an order of magnitude. This effect can be attributed to a lesser amount of noncondensable gas present in the bubble and a smaller area for heat and mass transfer. The lower water vapor entrapment in the bubble is compensated by the higher equilibrium composition of $OH^{\bullet}$ radicals for the temperature and pressure at collapse—which is ~2 orders of magnitude higher than the 200 micron bubble. On the whole, with other operating parameters remaining the same, smaller bubbles make a greater contribution to the sonochemical effects.

5.4. Effect of Cavitation Number. The effect of cavitation number on the bubble dynamics can be determined by comparing the simulation results depicted in Figures 1 and 5. As mentioned earlier, for cavitation number (C_i) = 1, the pressure at vena contracta falls to the vapor pressure of the liquid. For $C_i > 1$, the pressure at vena contracta is higher than the vapor pressure. Argon bubbles generated at vena contracta are in mechanical equilibrium with the flow, which means that the initial pressure in the bubble at vena contracta is $\sim(P_{vc} + 2\sigma/R_o)$. The higher the pressure at vena contracta, the higher is the initial pressure (i.e., higher argon content). Higher argon content reduces the compression ratio of the bubble at collapse, thus reducing the temperature and pressure reached during collapse. A higher pressure at vena contracta and its immediate vicinity also suppresses the effect of the negative oscillation of the turbulent pressure gradient, which is responsible for the expansion of the bubble, as mentioned earlier. Less expansion of the bubble causes a reduction in the water vapor that diffuses into the bubble. Thus, the subsequent entrapment of water vapor also decreases. Simulation results show that a small increment in the cavitation number, i.e., to 1.1 (for Figure 5) from 1 (for Figure 1), reduces the water vapor entrapment 4× and the equilibrium composition of $OH^{\bullet}$ radicals by 2 orders of magnitude.

6. Conclusions

In this paper, we have attempted to provide a numerical explanation to the sonochemical effect induced by hydrodynamic cavitation. Simulation results reveal that, as in acoustic cavitation, the phenomena of water vapor entrapment and radical formation during bubble collapse also occurs in the case of hydrodynamic cavitation. The entrapped water molecules undergo dissociation at the extreme temperature and pressure reached during collapse, as is shown by the equilibrium composition of the bubble contents. The $OH^{\bullet}$ radical is found to be the dominant radical species at the conditions of bubble collapse. The peak temperatures reached in the bubble during

Table 3. Equilibrium Composition (Mole Fraction) of Various Species at the Conditions of Pressure and Temperature Reached at First Compression of the Bubble

	parameter set for simulation				
species	set 1[a] ($T = 2994$ K, $P = 603.8$ atm, $N_{wc} = 6.8 \times 10^{14}$)	set 2[a] ($T = 3103$ K, $P = 683.8$ atm, $N_{wc} = 3.9 \times 10^{14}$)	set 3[a] ($T = 2368$ K, $P = 70.7$ atm, $N_{wc} = 9.8 \times 10^{12}$)	set 4[a] ($T = 1527$ K, $P = 14.2$ atm, $N_{wc} = 9.6 \times 10^{13}$)	set 5[a] ($T = 1774$ K, $P = 26.8$ atm, $N_{wc} = 1.2 \times 10^{14}$)
H_2O	9.5857×10^{-1}	9.4886×10^{-1}	9.8693×10^{-1}	9.9983×10^{-1}	9.9909×10^{-1}
H_2	1.9828×10^{-2}	2.4093×10^{-2}	6.8669×10^{-3}	1.0322×10^{-4}	5.2959×10^{-4}
$OH^{\bullet}$	1.3845×10^{-2}	1.7499×10^{-2}	3.4322×10^{-3}	2.0106×10^{-5}	1.5136×10^{-4}
O_2	6.4209×10^{-3}	7.6222×10^{-3}	2.5815×10^{-3}	4.6585×10^{-5}	2.2703×10^{-4}
$H^{\bullet}$	8.7615×10^{-4}	1.252×10^{-3}	1.3374×10^{-4}	6.5123×10^{-8}	1.2704×10^{-6}
$O^{\bullet}$	3.5666×10^{-4}	5.2359×10^{-4}	4.3797×10^{-5}	1.0493×10^{-8}	2.7453×10^{-7}
$HOO^{\bullet}$	7.547×10^{-5}	1.055×10^{-4}	5.8075×10^{-6}	6.0479×10^{-9}	8.9983×10^{-8}
H_2O_2	3.1992×10^{-5}	4.2752×10^{-5}	2.2075×10^{-6}	6.2858×10^{-9}	6.3448×10^{-8}
O_3	1.2002×10^{-8}	2.0258×10^{-8}	2.2352×10^{-10}	4.1437×10^{-15}	3.01×10^{-13}

[a] Values in parentheses are the conditions at the first compression of the bubble.

transient collapse in all the five sets, however, are less than those reported for in case of acoustic cavitation (~5000−7000 K).[38] This result can be explained in terms of the difference in the time scale of the bubble motion in hydrodynamic and acoustic cavitation, which varies directly with the time scale of pressure variation. The time scale of pressure variation in acoustic cavitation is of the order of microseconds (e.g., 50 μs for 20 kHz ultrasound), while that in hydrodynamic cavitation is of the order of milliseconds, as evident from the simulation parameters given in Table 2. Thus, greater heat transfer from bubble to the surroundings occurs during the bubble motion in hydrodynamic cavitation, lowering the peak temperature reached in the bubble.

The trends in the sonochemical effect produced by hydrodynamic cavitation evident from the simulation results can be summarized as follows:

1. A rise in the recovery pressure downstream of the orifice plate (which means greater energy input to the flow) does not raise the sonochemical effect, as one might expect. This is because the rise in the temperature and pressure attained during collapse, and hence the equilibrium composition of $OH^{\bullet}$ radicals, is compensated by the lesser entrapment of water vapor, due to the higher compression.

2. Smaller bubbles are found to be more productive of the sonochemical effects, as they undergo higher compression during collapse, attaining higher values of the temperatures and pressures reached during collapse at which the equilibrium composition of the $OH^{\bullet}$ radicals is higher.

3. The sonochemical effect is found to be critically sensitive to two parameters: the cavitation number (C_i) and the orifice-to-pipe-diameter ratio (β). A small rise in these parameters brings down the sonochemical effect by 1 order of magnitude.

Acknowledgment

V.S.M. would like to thank Dr. Rudiger Toegel (Physics of Fluids Group, Department of Physics, University of Twente, Netherlands) for valuable help in this work. V.S.M. also thanks Professor Andrea Prosperetti (Department of Mechanical Engineering, John Hopkins University, U.S.) and Dr. Brian Storey (Department of Mechanical Engineering, Franklin W. Olin College of Engineering, U.S.) for useful discussions.

Appendix A

Determination of Transport Parameters for Argon−Water Vapor Mixture. The transport properties (diffusion coefficient, D_{ij}, and coefficient of thermal conductivity, λ_{ij}) for the heat and mass transfer across the bubble have been determined using the Chapman−Enskog theory using the Lennard-Jones 12−6 potential. We give herewith only the final expressions for the transport parameters. More information, along with derivation for these expressions, can be found in Hirschfelder et al.[34] In the various notations that follow hereafter, subscript 1 represents water and subscript 2 represents argon. For the temperature T, we use the liquid temperature T_o.

Diffusion Coefficient. Diffusion coefficient of species 1 in the mixture of two species 1−2, to a first approximation, can be written as

$$D_{ij} = \frac{3}{8} \frac{\sqrt{\pi k T/\mu_{12}}}{n_{12} \pi {\sigma_{12}}^2 \, {\Omega_{12}}^{(1,1)*}}$$

m_1 and m_2 are the molecular masses of water and argon, respectively, and $\mu_{12} = (2m_1m_2)/(m_1 + m_2)$ is the reduced molecular mass of the two species. $n_{12} = n_1 + n_2$ is the joint concentration of the two species. σ_{12} is a parameter in the potential function characteristic of 1−2 interaction. It is approximated as $(\sigma_1 + \sigma_2)/2$, where σ_1 and σ_2 are the molecular diameters of water and argon. $\Omega_{12}^{(1,1)*}$ is a dimensionless correction of the first order that describes the deviation of the collisional cross section from the hard sphere cross section. Values of this parameter are given in Hirschfelder et al.[34] as a function of the reduced temperature of the two species:

$${T_{12}}^* = \sqrt{\left(\frac{T}{\epsilon/k}\right)_1 \left(\frac{T}{\epsilon/k}\right)_2}.$$

Values of the potential parameter (ϵ/k) in K are available in various texts.[34,39]

Thermal Conductivity. The binary mixture in the present case comprises a monatomic (argon) and a nonlinear polyatomic (water vapor) gas. The coefficient of thermal conductivity for a pure monatomic gas may be obtained from the rigorous kinetic theory. However, these formulas cannot be used for the polyatomic gases, as the effect of the internal degrees of freedom on the thermal conductivity is considerable. The best way to correct the monatomic gas formulas so as to make them applicable to the polyatomic gases is to use the Eucken correction.

The coefficient of thermal conductivity for a monatomic gas is given as

$$\lambda = \frac{15}{4} \frac{k}{m} \eta$$

where m is the molecular mass and η is the coefficient of

viscosity, given as

$$\eta = \frac{5}{16}\frac{\sqrt{\pi\, mkT}}{\pi\sigma^2\Omega^{(2,2)*}}$$

For a polyatomic molecule, the above expression is replaced as

$$\lambda_{\text{Eucken}} = \frac{15}{4}\frac{k}{m}\eta\left(\frac{4}{15}\frac{C_v}{Nk} + \frac{3}{5}\right)$$

It could be noted for a monatomic molecule $C_v = 3Nk/2$ (heat capacity per mole), and the corrected expression with the Eucken factor reverts to the first expression. Using the above formulas, the thermal conductivity for the mixture of argon and water vapor is calculated as follows. We first define a quantity λ_{12} such as the following:

$$\lambda_{12} = \frac{25}{32}\left(\frac{\sqrt{\pi kT/\mu_{12}}}{\pi\sigma_{12}{}^2\Omega_{12}{}^{(2,2)*}T_{12}{}^*}\right)\frac{3}{2}k$$

$\Omega_{12}{}^{(2,2)*}$ is again a dimensionless correction for the first order, similar to the quantity $\Omega_{12}{}^{(1,1)*}$ defined earlier. In terms of this quantity, and the thermal conductivities of pure components, viz. water (λ_1) and argon (λ_2), both being calculated using the formula for the monatomic gas stated above, a new quantity λ_{mon} is calculated as

$$\lambda_{\text{mon}} = \frac{1+Z}{X+Y}$$

X, Y, and Z are defined in terms of the mole fractions of two components, x_1 and x_2, as

$$X = \frac{x_1{}^2}{\lambda_1} + \frac{2x_1x_2}{\lambda_{12}} + \frac{x_2{}^2}{\lambda_2}$$

$$Y = \frac{x_1{}^2}{\lambda_1}U_1 + \frac{2x_1x_2}{\lambda_{12}}U_Y + \frac{x_2{}^2}{\lambda_2}U_2$$

$$Z = x_1{}^2U_1 + 2x_1x_2U_Z + x_2{}^2U_2$$

The quantities U_1, U_2, U_Y, and U_Z are given as

$$U_1 = \frac{4}{15}A_{12}{}^* - \frac{1}{12}\left(\frac{12}{5}B_{12}{}^* + 1\right)\frac{m_1}{m_2} + \frac{1}{2}\frac{(m_1-m_2)^2}{m_1m_2}$$

$$U_2 = \frac{4}{15}A_{12}{}^* - \frac{1}{12}\left(\frac{12}{5}B_{12}{}^* + 1\right)\frac{m_2}{m_1} + \frac{1}{2}\frac{(m_2-m_1)^2}{m_1m_2}$$

$$U_Y = \frac{4}{15}A_{12}{}^*\left[\frac{(m_1+m_2)^2}{4m_1m_2}\right]\frac{\lambda_{12}{}^2}{\lambda_1\lambda_2} - \frac{1}{12}\left(\frac{12}{5}B_{12}{}^* + 1\right) - \frac{5}{32A_{12}{}^*}\left(\frac{12}{5}B_{12}{}^* - 5\right)\frac{(m_1-m_2)^2}{m_1m_2}$$

$$U_Z = \frac{4}{15}A_{12}{}^*\left\{\left[\frac{(m_1+m_2)^2}{4m_1m_2}\right]\left(\frac{\lambda_{12}}{\lambda_1} + \frac{\lambda_{12}}{\lambda_2}\right) - 1\right\} - \frac{1}{12}\left(\frac{12}{5}B_{12}{}^* + 1\right)$$

The quantities $A_{12}{}^*$ and $B_{12}{}^*$ are functions of the quantities Ω defined earlier and are written as

$$A_{12}{}^* = \frac{\Omega^{(2,2)*}}{\Omega^{(1,1)*}} \text{and} \quad B_{12}{}^* = \frac{5\,\Omega^{(1,2)*} - 4\Omega^{(1,3)*}}{\Omega^{(1,1)*}}.$$

Values of $A_{12}{}^*$ and $B_{12}{}^*$ are tabulated in Hirschfelder et al.[34] as a function of the reduced temperature $T^* = T/(\epsilon/k)$.

After determining λ_{mon}, the coefficient of the thermal conductivity for the mixture is determined using the correlation

$$\lambda_{ij} = \lambda_{\text{mon}}(x_1E_1 + x_2E_2)$$

where E_1 and E_2 are the ratios of the experimental value and the theoretical value of thermal conductivity, determined by the formula for a monatomic gas. $E_2 \approx 1$, because argon is a monatomic gas and the experimental value of its thermal conductivity is almost equal to the value determined with the formula. For water vapor, E_1 is calculated as

$$E_1 = \frac{\lambda_{\text{exptl}}}{\lambda_1}$$

For the experimental value of the thermal conductivity of water, we use the correlation given by Reid et al.:[39]

$$\lambda_{\text{exptl}} = (7.341\times10^{-3}) - (1.013\times10^{-5})T + (1.801\times10^{-7})T^2 - (9.1\times10^{-11})T^3$$

where T is in K and λ in W/(m K).

Nomenclature

A = frequency factor in Arrhenius equation
c = velocity of sound in water
C_{i} = cavitation number
$C_{p,\text{Ar}}$ = heat capacity at constant pressure for argon
$C_{p,\text{mix}}$ = heat capacity at constant pressure for binary mixture
$C_{p,\text{W}}$ = heat capacity at constant pressure for water
C_v = heat capacity at constant volume
$C_{v,\text{Ar}}$ = heat capacity at constant volume for argon
$C_{v,\text{W}}$ = heat capacity at constant volume for water vapor
C_{W} = concentration of water molecules in the bubble core
C_{W0} = initial concentration of water molecules in the bubble
C_{WR} = concentration of water molecules at the bubble wall
d_{c} = diameter of conduit
D_{ij} = binary diffusion coefficient for argon−water vapor mixture
E = total energy of bubble contents
E_a/k = activation temperature (in Arrhenius equation)
f_{T} = frequency of turbulent fluctuating velocity
h = van der Waals hard core radius
h_{W} = specific enthalpy of water molecules
k = Boltzmann constant
k_{r} = specific reaction rate constant (defined by Arrhenius equation)
k_{f} = specific reaction rate constant for forward radical reaction
k_{b} = specific reaction rate constant for backward radical reaction
l = length scale of eddy

L' = distance of pressure recovery downstream of the orifice plate
l_{diff} = diffusion length (mass diffusion)
l_{th} = diffusion length (thermal diffusion)
N = Avogadro number
N_{Ar} = number of argon molecules in the bubble
N_{tot} = total number of molecules in the bubble
N_W = number of water molecules in the bubble
N_{wc} = number of water molecules trapped in the bubble at collapse
P_2 = recovered pressure of flow downstream of orifice plate
P_i = pressure inside the bubble
P_t = instantaneous bulk pressure in the medium driving bubble motion
P_v = vapor pressure of water at ambient temperature T_o
P_{vc} = pressure in the flow at vena contracta
Q = heat transferred across bubble wall
R = bubble radius at any time t
r = radial coordinate
R_o = initial bubble radius
T = instantaneous temperature of the bubble
t = time
t_{osc} = time scale of bubble dynamics
t_{cond} = time scale for water vapor condensation at the bubble wall
t_{diff} = time scale for water vapor diffusion to the bubble wall
t_{react} = time scale of radical reaction occurring in the bubble
T_o = ambient temperature or temperature of the bulk liquid
$\bar{u}'$ = turbulent fluctuating velocity
U = mean velocity of the flow downstream of the orifice plate
U_o = mean velocity of flow at vena contracta
U_p = velocity through pipe
U_t = instantaneous mean velocity of flow downstream of orifice plate
U_W = specific energy of the water molecules
W = work done by the bubble

Greek Letters

ρ_L = density of the liquid
ν = kinematic viscosity of the liquid
σ = surface tension of the liquid
σ_a = accommodation coefficient for the water vapor at the bubble surface
γ = polytropic index of the bubble contents
κ = thermal diffusivity
ω = angular frequency
λ_{ij} = thermal conductivity of the binary (argon−water vapor) mixture
κ_{ij} = thermal diffusivity of the binary (argon−water vapor) mixture
ρ_{mix} = molecular density of the binary (argon−water vapor) mixture
ρ_{Ar} = molecular density of argon
ρ_W = molecular density of water vapor
θ_i = characteristic vibrational temperatures for the water molecule
β = orifice to pipe diameter ratio
τ = time for full pressure recovery downstream of orifice plate

Literature Cited

(1) Suslick, K. S. *Ultrasound: Its Physical, Chemical and Biological Effects*; VCH: New York, 1988.

(2) Mason, T. J.; Lorimer, J. P. *Sonochemistry: Theory, Applications and Uses of Ultrasound in Chemistry*; Ellis Horwood: New York, 1989.

(3) Shah, Y. T.; Pandit, A. B.; Moholkar, V. S. *Cavitation Reaction Engineering*; Plenum Publishers: New York, 1999.

(4) Suslick, K. S.; Mdleleni, M. M.; Reis, J. T. Chemistry Induced by Hydrodynamic Cavitation. *J. Acoust. Soc. Am.* **1997**, *119*, 9303.

(5) Senthil Kumar, P.; Siva Kumar, M.; Pandit, A. B. Experimental Quantification of Chemical Effects of Hydrodynamic Cavitation. *Chem. Eng. Sci.* **2000**, *55*, 1633.

(6) Vichare, N. P.; Gogate, P. R.; Pandit, A. B. Optimization of Hydrodynamic Cavitation Using Model Reaction. *Chem. Eng. Technol.* **2000**, *23*, 683.

(7) Hart, E. J.; Henglein, A. Free Radical and Free Atom Reactions in the Sonolysis of Aqueous Iodide and Formate Solutions. *J. Phys. Chem.* **1985**, *89*, 4342.

(8) Kamath, V.; Prosperetti, A.; Egolfopoulos, F. N. A Theoretical Study of Sonoluminescence. *J. Acoust. Soc. Am.* **1993**, *94*, 248.

(9) Prasad Naidu, D. V.; Rajan, R.; Kumar, R.; Gandhi, K. S.; Arakeri, V. H.; Chandrasekaran, S. Modeling of a Batch Sonochemical Reactor. *Chem. Eng. Sci.* **1994**, *49*, 377.

(10) Sochard, S.; Wilhelm, A. M.; Delmas, H. Modeling of Free Radicals Production in a Collapsing Gas-Vapor Bubble. *Ultrasonics Sonochemistry* **1997**, *4*, 77.

(11) Yasui, K. Alternative Model for Single-Bubble Sonoluminescence. *Phys. Rev. E* **1997**, *56*, 6750.

(12) Yasui, K. Chemical Reactions in a Sonoluminescing Bubble. *J. Phys. Soc. Jpn.* **1997**, *66*, 2911.

(13) Gong, C.; Hart, D. P. Ultrasound Induced Cavitation and Sonochemical Yields. *J. Acoust. Soc. Am.* **1998**, *104*, 2675.

(14) Colussi, A. J.; Weavers, L. K.; Hoffmann, M. R. Chemical Bubble Dynamics and Quantitative Sonochemistry. *J. Phys. Chem. A* **1998**, *102*, 6927.

(15) Colussi, A. J.; Hoffmann, M. R. Vapor Supersaturation in Collapsing Bubbles. Relevance to Mechanisms of Sonochemistry and Sonoluminescence. *J. Phys. Chem. A* **1999**, *103*, 11336.

(16) Moss, W. C.; Young, D. A.; Harte, J. A.; Levalin, J. L.; Rozsnyai, B. F.; Zimmerman, G. B.; Zimmerman, I. H. Computed Optical Emissions from Sonoluminescing Bubbles. *Phys. Rev. E* **1999**, *59*, 2956.

(17) Storey, B. D.; Szeri, A. J. Water Vapor, Sonoluminescence and Sonochemistry. *Proc. R. Soc. London, Ser. A* **2000**, *456*, 1685.

(18) Storey, B. D.; Szeri, A. J. A Reduced Model of Cavitation Physics for use in Sonochemistry. *Proc. R. Soc. London, Ser. A* **2001**, *457*, 1685.

(19) Toegel, R.; Gompf, B.; Pecha, R.; Lohse, D. Does Water Vapor Prevent Upscaling Sonoluminescence. *Phys. Rev. Lett.* **2000**, *85*, 3165.

(20) Flynn, H. G. Physics of Acoustic Cavitation in Liquids. In *Physical Acoustics*;Mason, W. P., Ed.; Academic Press: New York, 1964; pp 57−172.

(21) Eames, I. W.; Marr, N. J.; Sabir, H. The Evaporation Coefficient of Water: A Review. *Int. J. Heat Mass Transfer* **1997**, *40*, 2963.

(22) Kwak, H.-Y.; Yang, H. An Aspect of Sonoluminescence from Hydrodynamic Theory. *J. Phys. Soc. Jpn.* **1995**, *64*, 1980.

(23) Kwak, H.-Y.; Na, J. H. Physical Processes for Single Bubble Sonoluminescence. *J. Phys. Soc. Jpn.* **1997**, *66*, 3074.

(24) Kwak, H.-Y.; Na, J.-H. Hydrodynamic Solutions for Sonoluminescing Gas Bubble. *Phys. Rev. Lett.* **1996**, *77*, 4454.

(25) Fujikawa, S.; Akamatsu, T. Effects of the Nonequilibrium Condensation of Vapor on the Pressure Wave Produced by the Collapse of a Bubble in a Liquid. *J. Fluid Mech.* **1980**, *97*, 481.

(26) Morrison, G. L.; DeOtte, R. E., Jr.; Nail, G. H.; Panak, D. L. Mean Velocity and Turbulence Fields Inside a $\beta = 0.5$ Orifice Flowmeter. *AIChE J.* **1993**, *39*, 745.

(27) Moholkar, V. S.; Pandit, A. B. Bubble Behavior in Hydrodynamic Cavitation: Effect of Turbulence. *AIChE J.* **1997**, *43*, 1641.

(28) Moholkar, V. S.; Pandit, A. B. Modeling of Hydrodynamic Cavitation Reactors: A Unified Approach. *Chem. Eng. Sci.* **2001**, *56*, 6295.

(29) Prosperetti, A.; Lezzi, A. Bubble Dynamics in a Compressible Liquid. Part 1. First-Order Theory. *J. Fluid Mech.* **1986**, *168*, 457.

(30) Brennen, C. E. *Cavitation and Bubble Dynamics*; Oxford University Press: Oxford, U.K., 1995.

(31) Plesset, M. S.; Prosperetti, A. Bubble Dynamics and Cavitation. *Annu. Rev. Fluid Mech.* **1977**, *9*, 145.

(32) Hilgenfeldt, S.; Lohse, D.; Brenner, M. P. Phase Diagrams for Sonoluminescing Bubbles. *Phys. Fluids* **1996**, *8*, 2808.

(33) Crank, J. *The Mathematics of Diffusion*; Clarendon Press: Oxford, U.K., 1975.

(34) Hirschfelder, J. O.; Curtiss, C. F.; Bird, R. B. *Molecular Theory of Gases and Liquids*; Wiley: New York, 1954.

(35) Yan, Y.; Thorpe, R. B.; Pandit, A. B. Cavitation Noise and Its Suppression by Air in Orifice Flow. Presented at *Proc. Intl. Symp. Flow Induced Vibration and Noise* (*ASME*), Chicago, 1988.

(36) Press, W. H.; Teukolsky, S. A.; Flannery, B. P.; Vetterling, W. T. *Numerical Recipes*; Cambridge University Press: New York, 1992.

(37) Eriksson, G. Thermodynamic Studies of High-Temperature Equilibria. XII. SOLGAMIX, A Computer Program for Calculation of Equilibrium Composition in Multiphase Systems. *Chemica Scripta* **1975**, *8*, 100.

(38) Brenner, M. P.; Hilgenfeldt, S.; Lohse, D. Single Bubble Sonoluminescence. *Rev. Mod. Phys.* **2002**, *74*, 425.

(39) Reid, R. C.; Prausnitz, J. M.; Poling, B. E. *Properties of Gases and Liquids*; McGraw-Hill: New York, 1987.

(40) Lu, X.; Prosperetti, A.; Toegel, R.; Lohse, D. Harmonic Enhancement of Single Bubble Sonoluminescence. *Phys. Rev. E* **2003**, *67*, 56310.

Received for review July 18, 2005
Revised manuscript received December 2, 2005
Accepted December 12, 2005

IE050839T